Electronic Supplementary Material (ESI) for Journal of Materials Chemistry A.

Supporting Information for:

Antisolvent processing of lead halide perovskite thin films studied by in-situ X-ray diffraction

Karsten Bruening[1], Christopher J. Tassone[1]

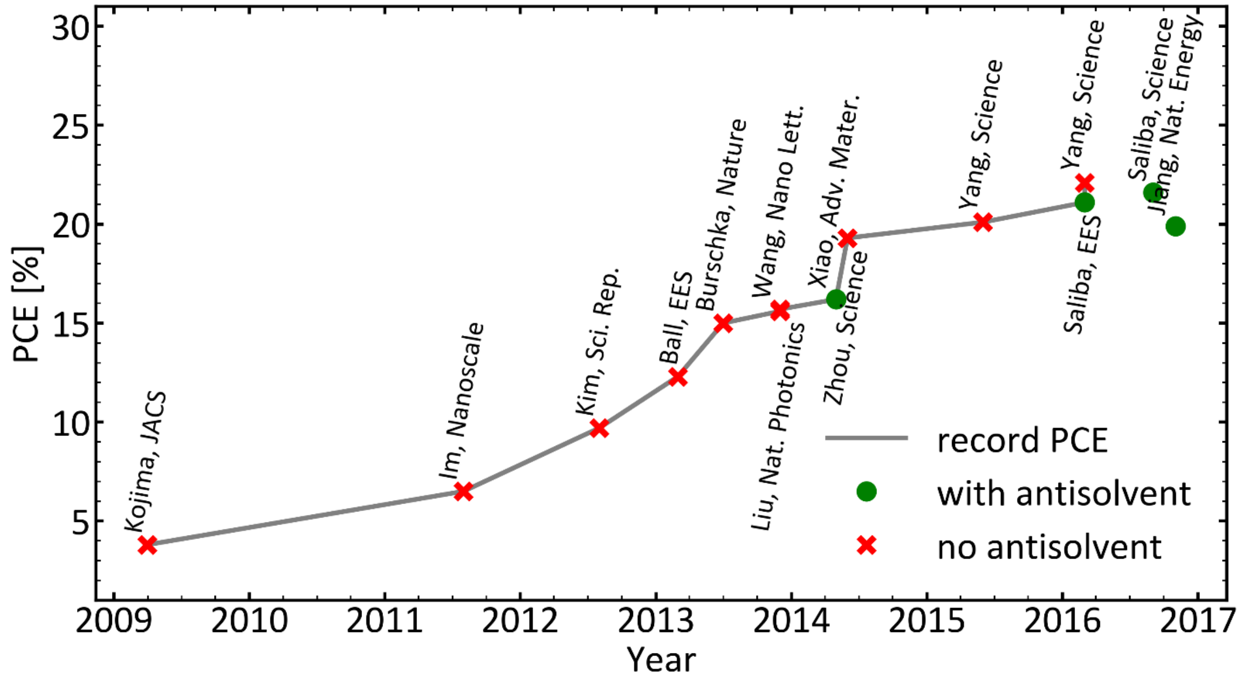

Figure S1 | Power conversion efficiency of record and select antisolvent-produced perovskite devices over time. See Table S1 for references.

Table S1 | References for Figure S1.

Author	Journal	Reference
Kojima	JACS	1
Im	Nanoscale	2
Kim	Sci. Rep.	3
Ball	EES	4
Burschka	Nature	5
Wang	Nano Lett.	6
Liu	Nat. Photonics	7
Xiao	Adv. Mater.	8
Zhou	Science	9
Yang	Science	10
Saliba	EES	11
Yang	Science	12

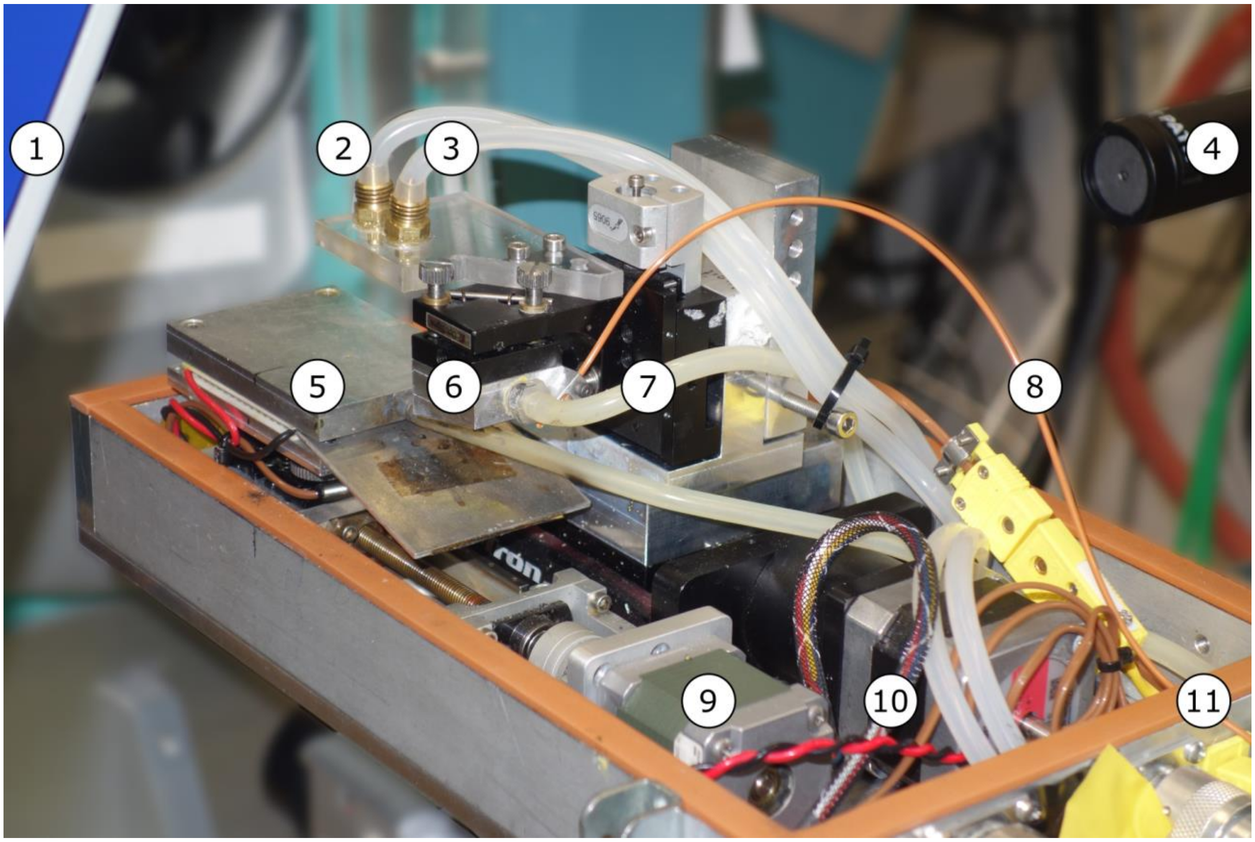

Figure S2 | Photo of experimental setup. 1: X-ray area detector; 2: antisolvent nozzle; 3: gas nozzle; 4: X-ray aperture; 5: table to mount substrate; 6: blade; 7: vacuum line to hold substrate and blade; 8: ink feed line; 9: motorized linear stage to scan film in X-ray beam; 10: motorized linear stage to move blade; 11: seal to contain inert atmosphere (lid not shown).

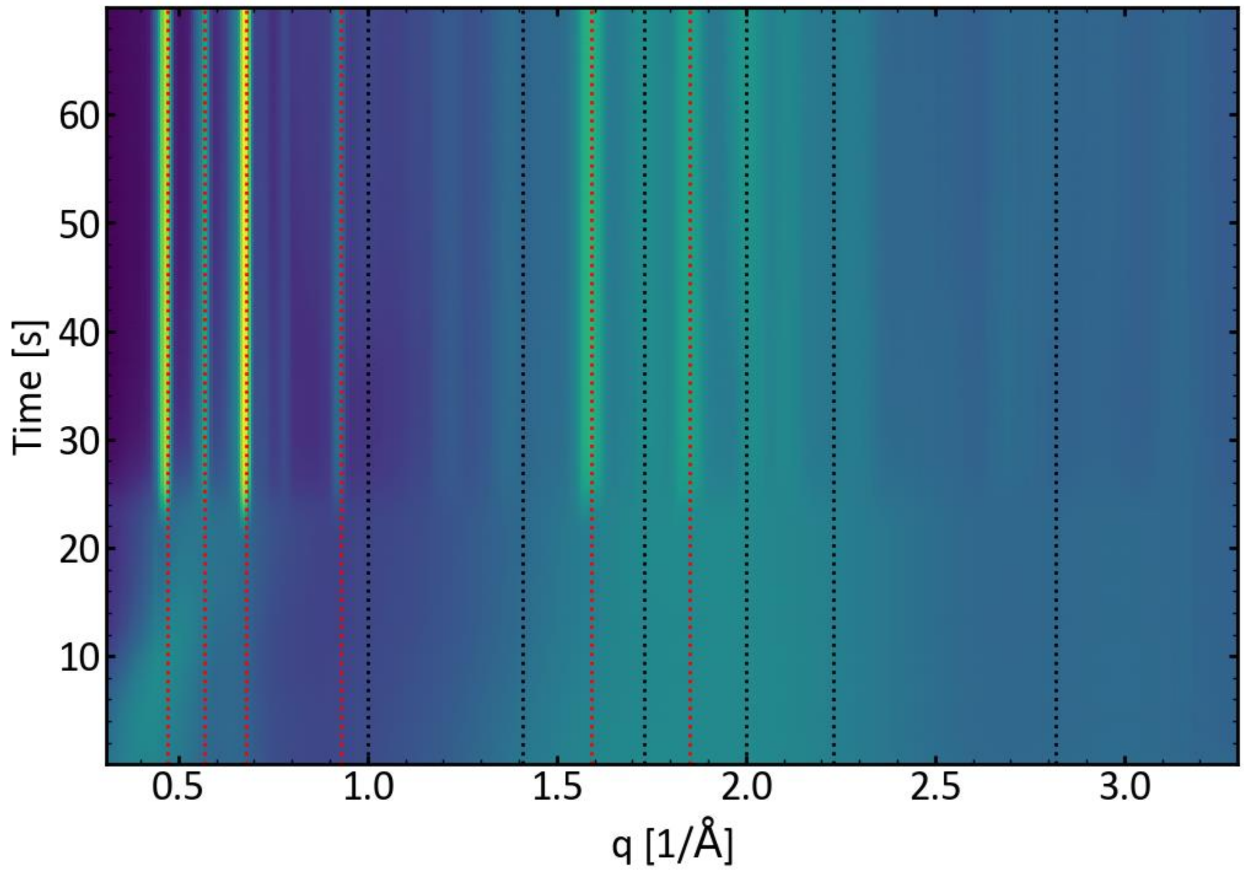

Figure S3 | *In situ* XRD during drying of blade coated film at room temperature (DMF). The red and black dashed lines indicate the calculated peak positions for the intermediate and perovskite phase, respectively. The calculated peak positions are based on jp7b08468_si_002.cif.[13]

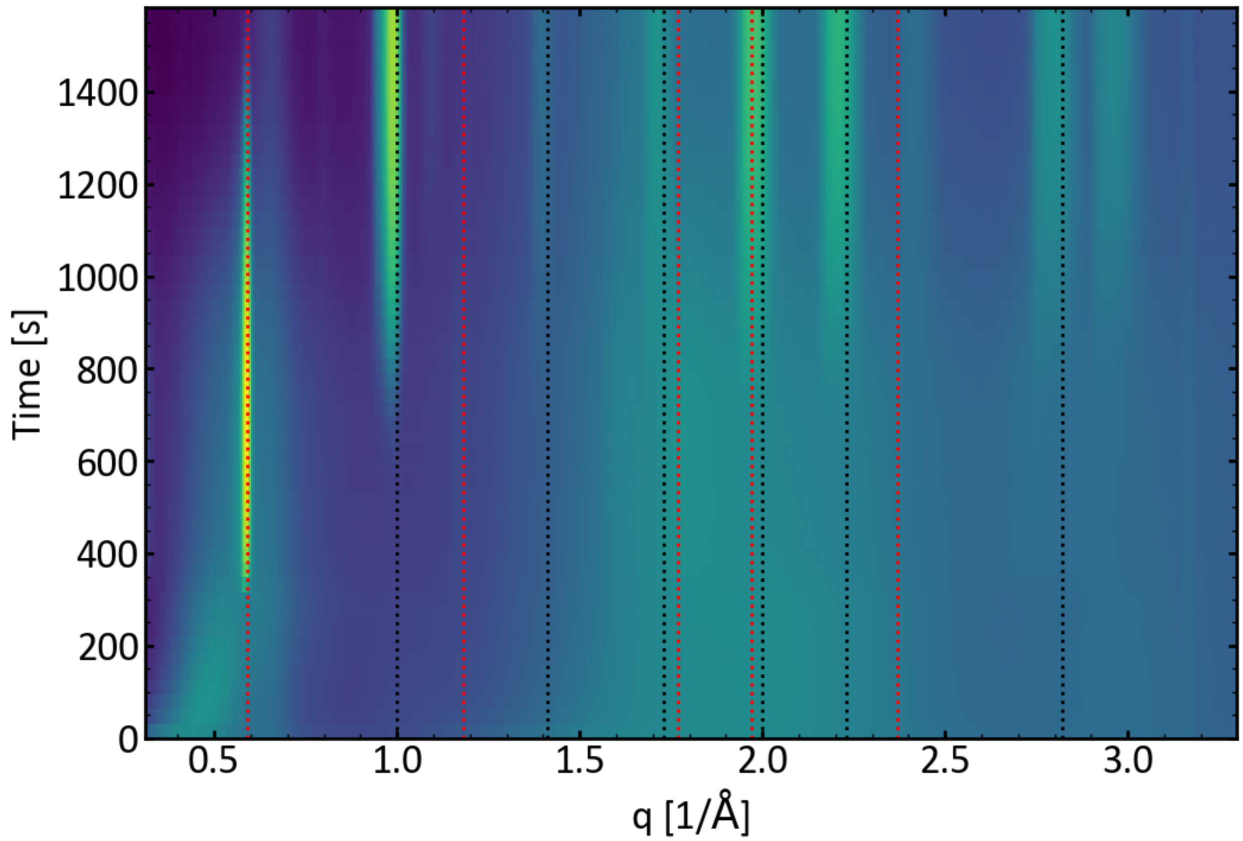

Figure S4 | *In situ* XRD during drying of blade coated film at room temperature (NMP). The red and black dashed lines indicate the calculated peak positions for the intermediate and perovskite phase, respectively. The calculated peaks are based on http://www.crystallography.net/cod/1011333.html with the _cell_length_c parameter modified to 10.65 Å.

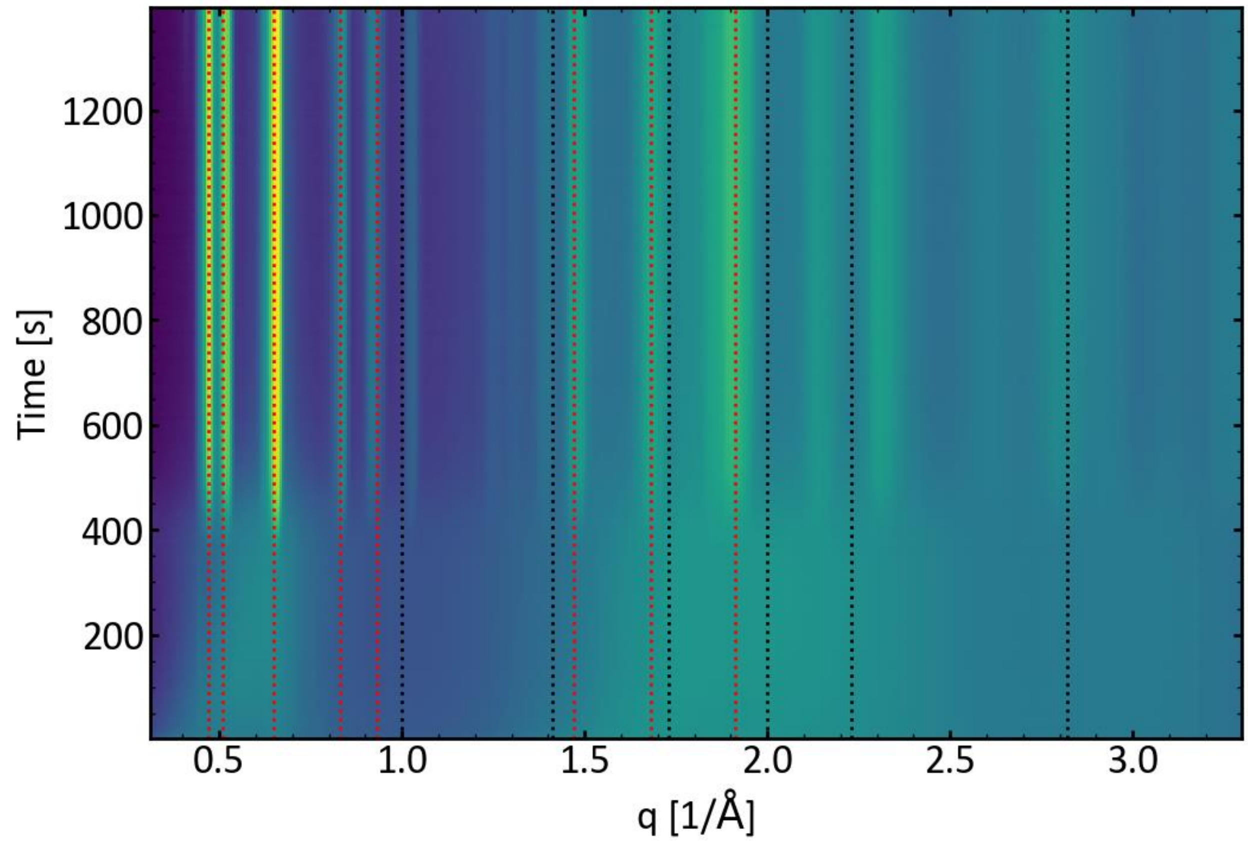

Figure S5 | *In situ* XRD during drying of blade coated film at room temperature (DMSO). The red and black dashed lines indicate the calculated peak positions for the intermediate and perovskite phase, respectively. The calculated peaks are based on ja5b10599_si_006 INT-3.cif [14], which is equivalent to c5nr02866c2.cif[15].

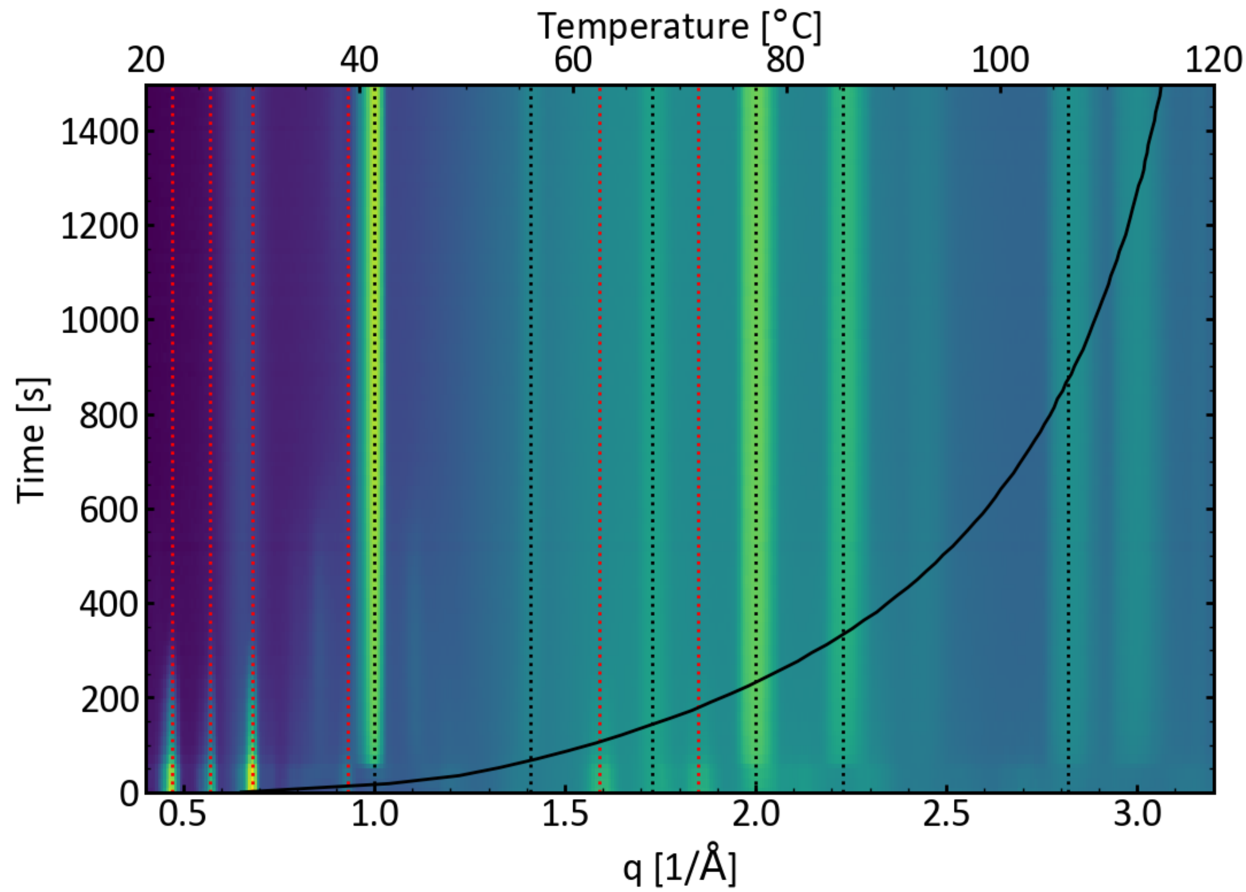

Figure S6 | *In situ* XRD during drying and heating of blade coated film (DMF, no CB). The red and black dashed lines indicate the calculated peak positions for the intermediate and perovskite phase, respectively. The solid black line shows the temperature (top abscissa).

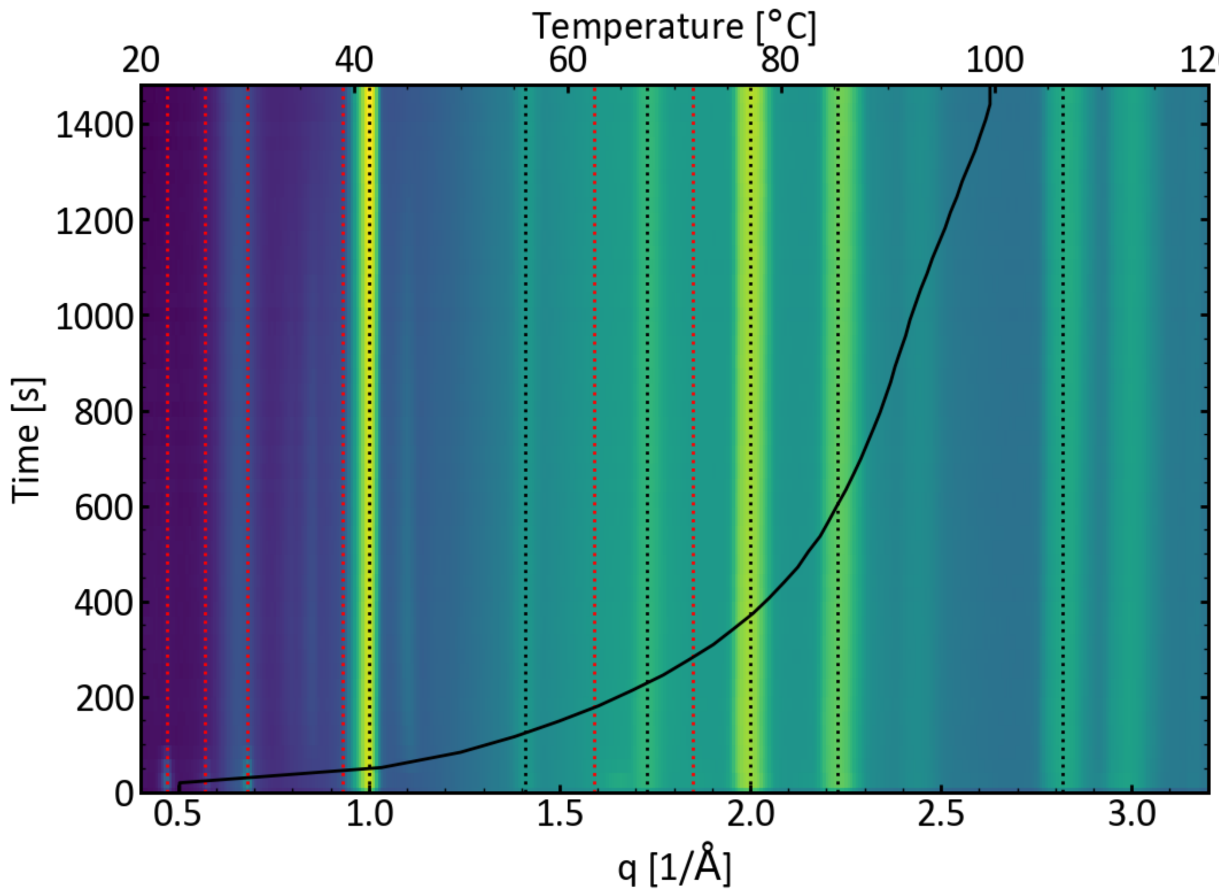

Figure S7 | *In situ* XRD during drying and heating of blade coated film (DMF, CB added at 0 min). The red and black dashed lines indicate the calculated peak positions for the intermediate and perovskite phase, respectively. The solid black line shows the temperature (top abscissa).

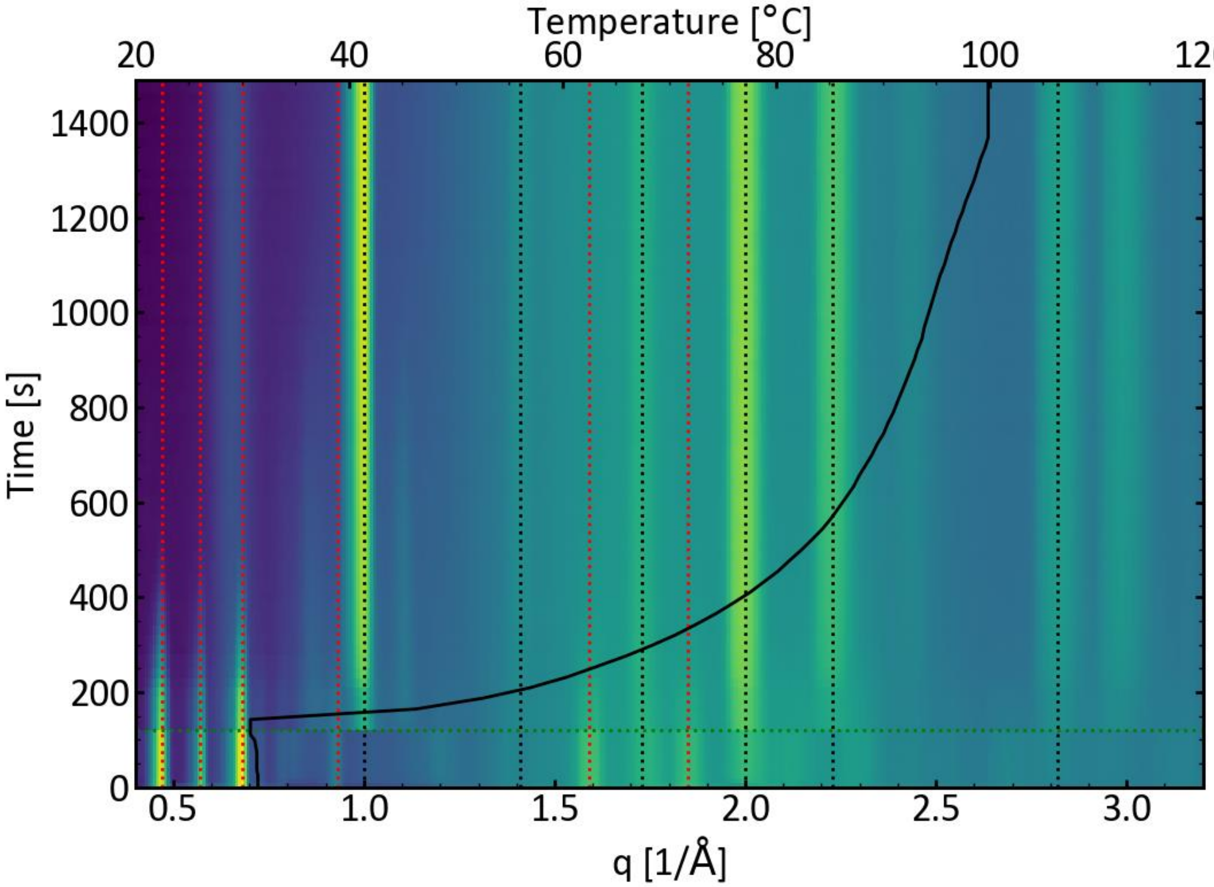

Figure S8 | *In situ* XRD during drying and heating of blade coated film (DMF, CB added at 2 min). The red and black dashed lines indicate the calculated peak positions for the intermediate and perovskite phase, respectively. The green dashed line marks the addition of chlorobenzene. The solid black line shows the temperature (top abscissa).

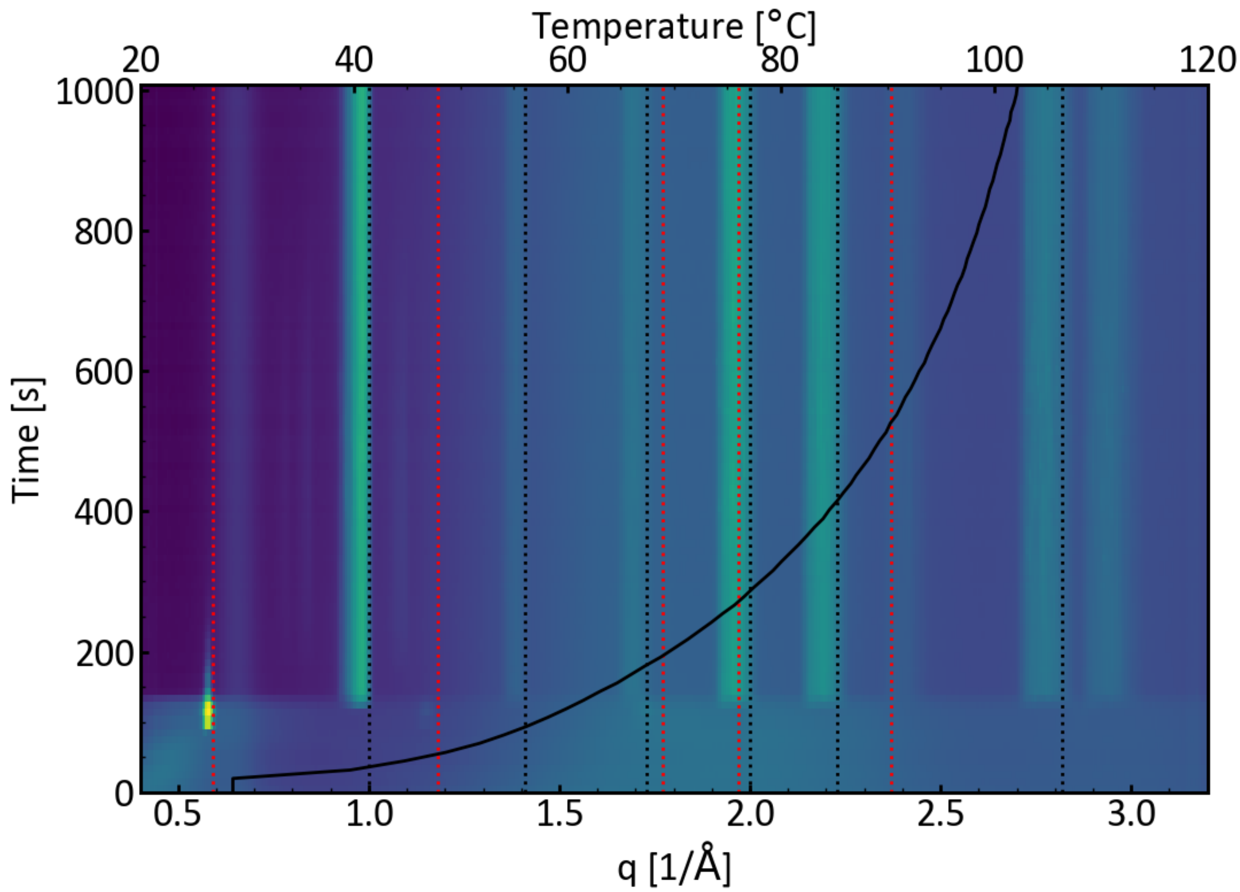

Figure S9 | *In situ* XRD during drying and heating of blade coated film (NMP, no CB). The red and black dashed lines indicate the calculated peak positions for the intermediate and perovskite phase, respectively. The solid black line shows the temperature (top abscissa).

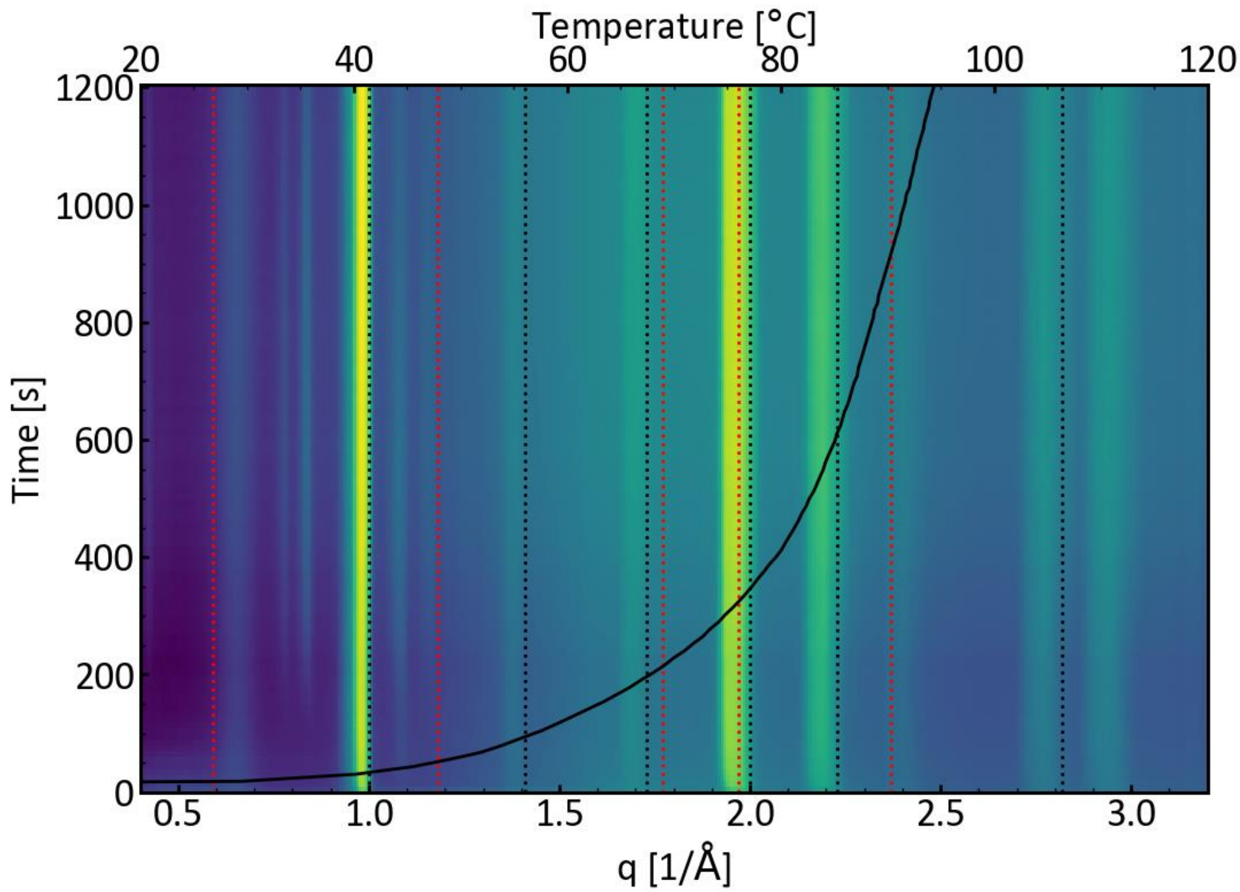

Figure S10 | *In situ* XRD during drying and heating of blade coated film (NMP, CB added at 0 min). The red and black dashed lines indicate the calculated peak positions for the intermediate and perovskite phase, respectively. The solid black line shows the temperature (top abscissa).

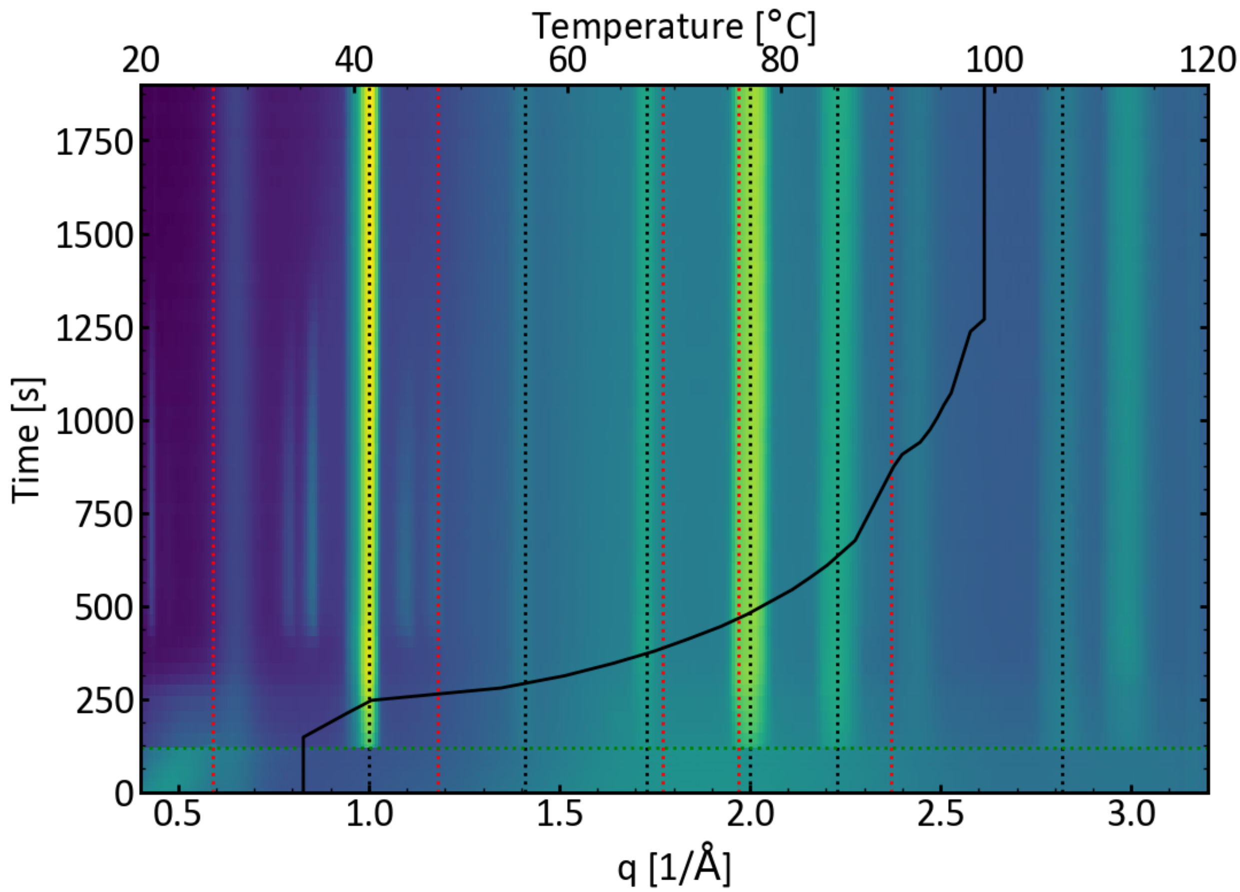

Figure S11 | *In situ* XRD during drying and heating of blade coated film (NMP, CB added at 2 min). The red and black dashed lines indicate the calculated peak positions for the intermediate and perovskite phase, respectively. The green dashed line marks the addition of chlorobenzene. The solid black line shows the temperature (top abscissa).

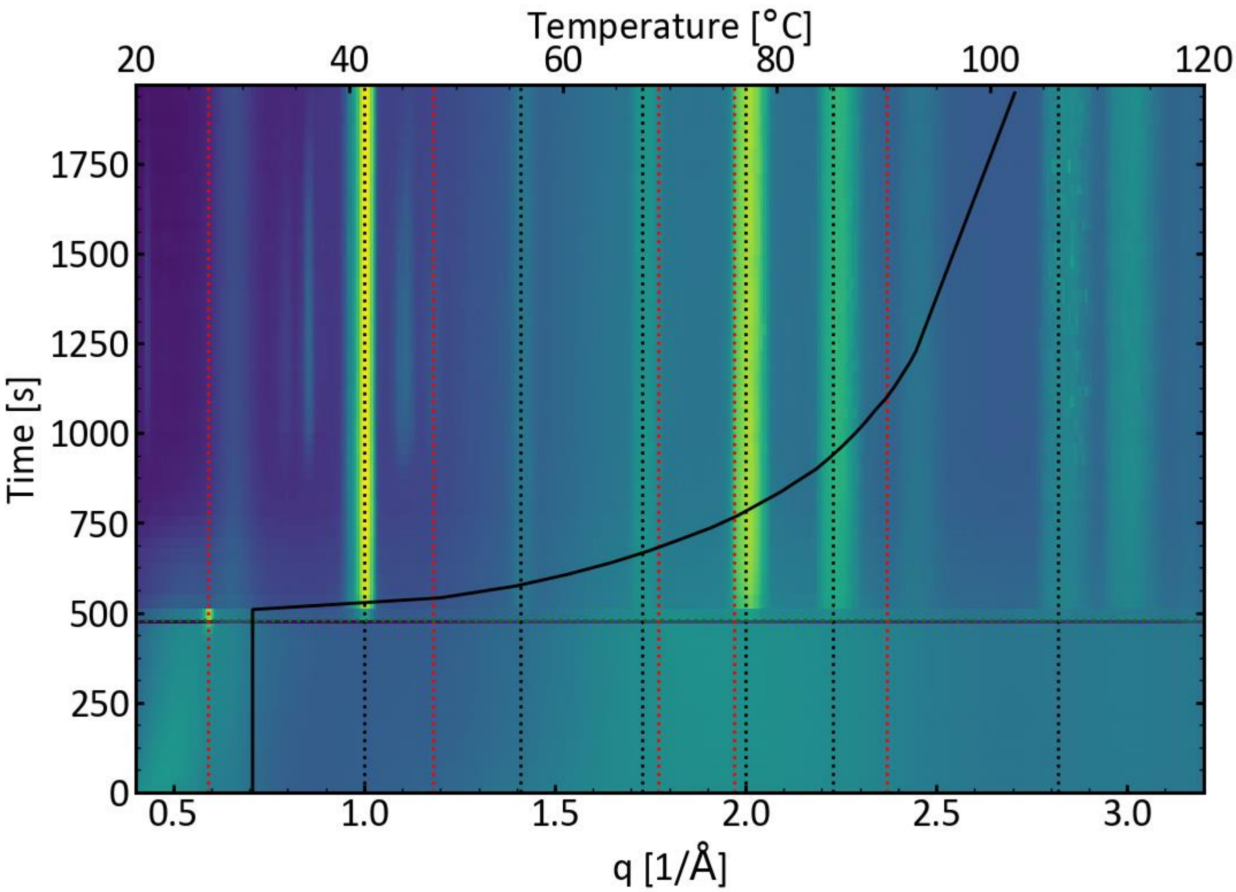

Figure S12 | *In situ* XRD during drying and heating of blade coated film (NMP, CB added at 8 min). The red and black dashed lines indicate the calculated peak positions for the intermediate and perovskite phase, respectively. The green dashed line marks the addition of chlorobenzene. The solid black line shows the temperature (top abscissa).

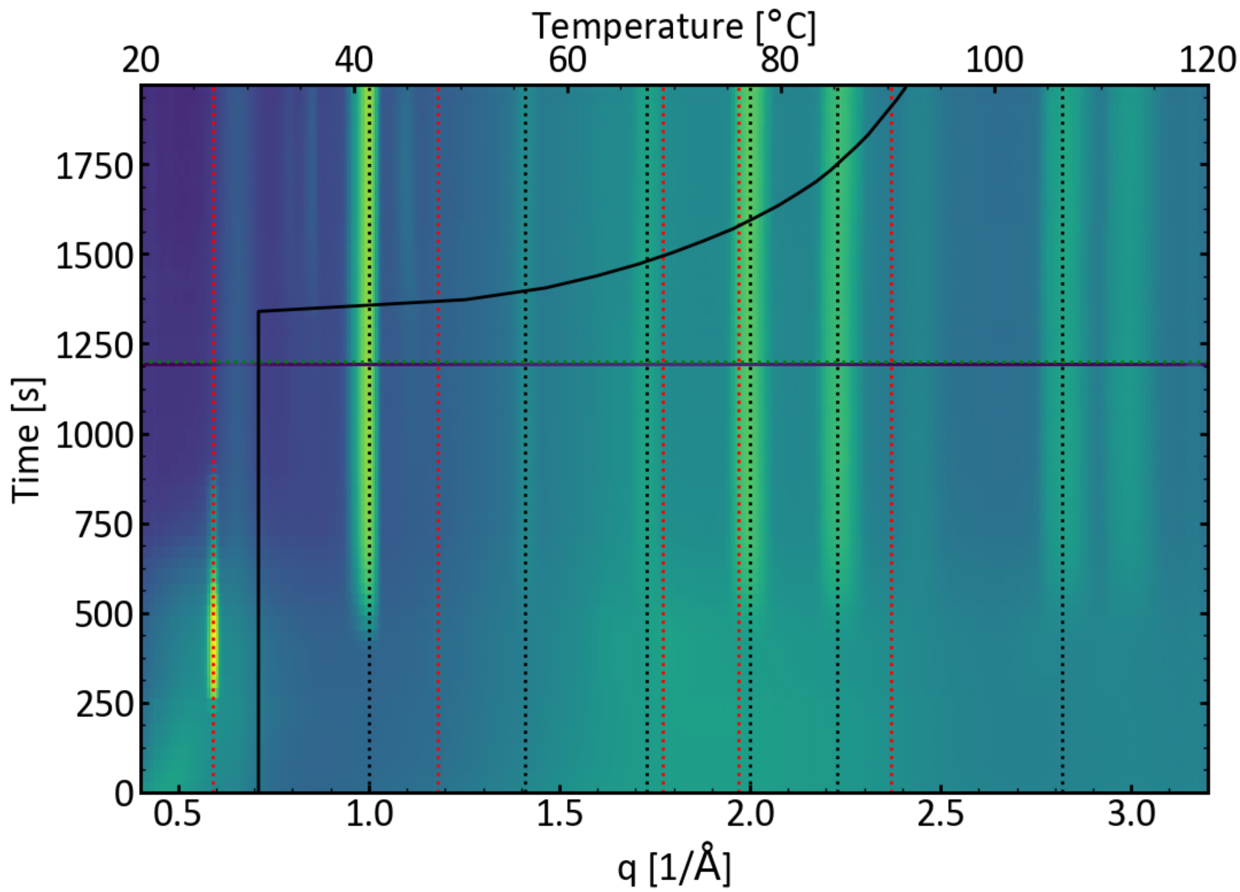

Figure S13 | *In situ* XRD during drying and heating of blade coated film (NMP, CB added at 20 min). The red and black dashed lines indicate the calculated peak positions for the intermediate and perovskite phase, respectively. The green dashed line marks the addition of chlorobenzene. The solid black line shows the temperature (top abscissa).

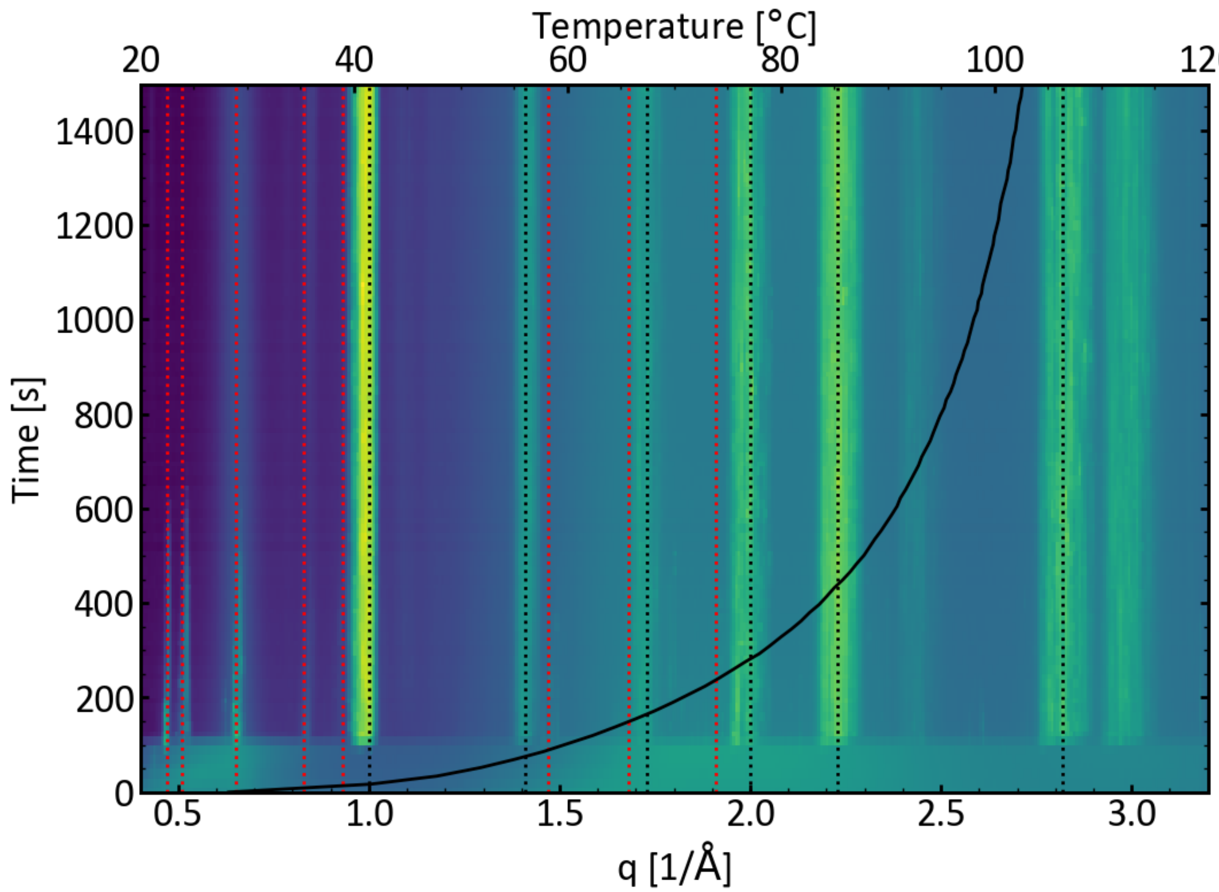

Figure S14 | *In situ* XRD during drying and heating of blade coated film (DMSO, no CB). The red and black dashed lines indicate the calculated peak positions for the intermediate and perovskite phase, respectively. The solid black line shows the temperature (top abscissa).

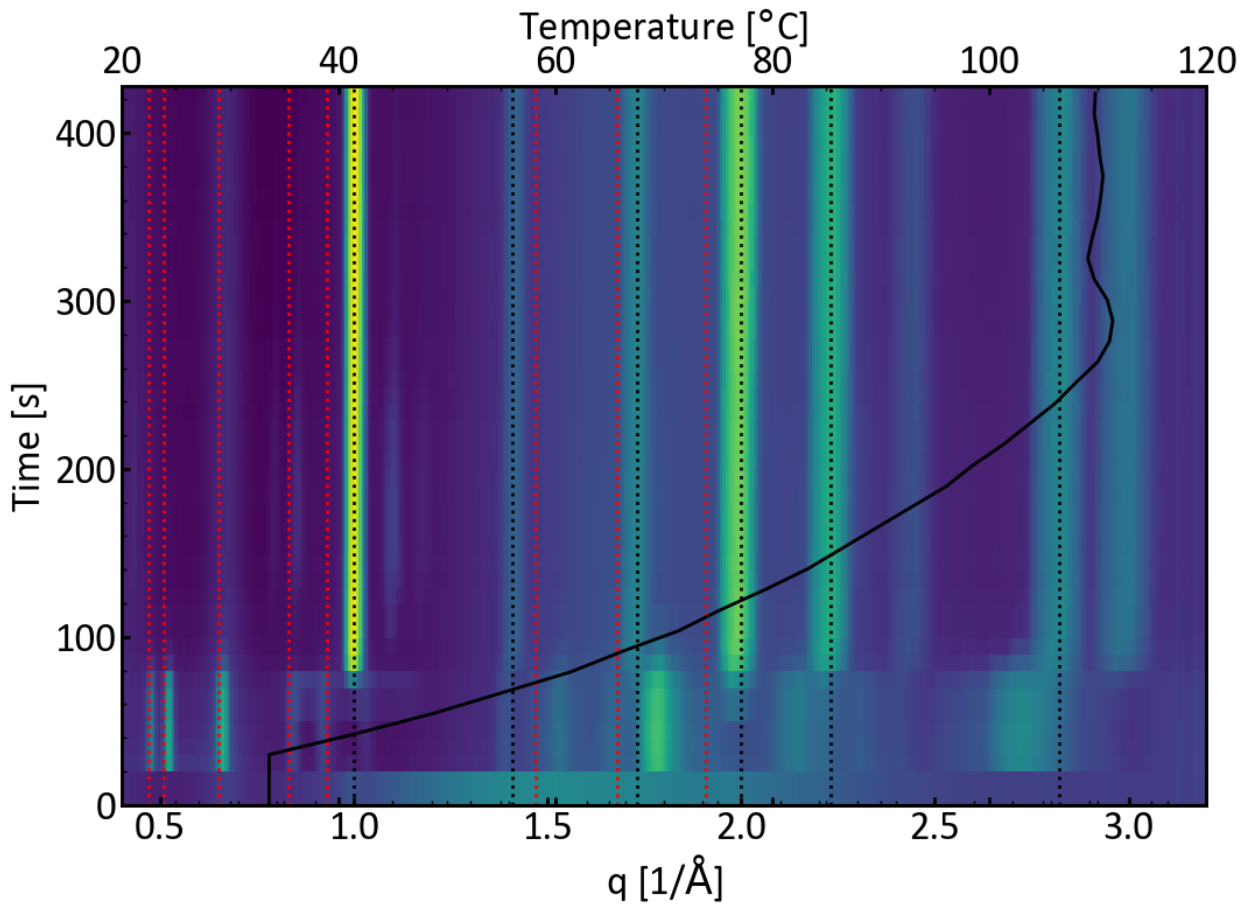

Figure S15 | *In situ* XRD during drying and heating of blade coated film (DMSO, CB added at 0 min). The red and black dashed lines indicate the calculated peak positions for the intermediate and perovskite phase, respectively. The solid black line shows the temperature (top abscissa).

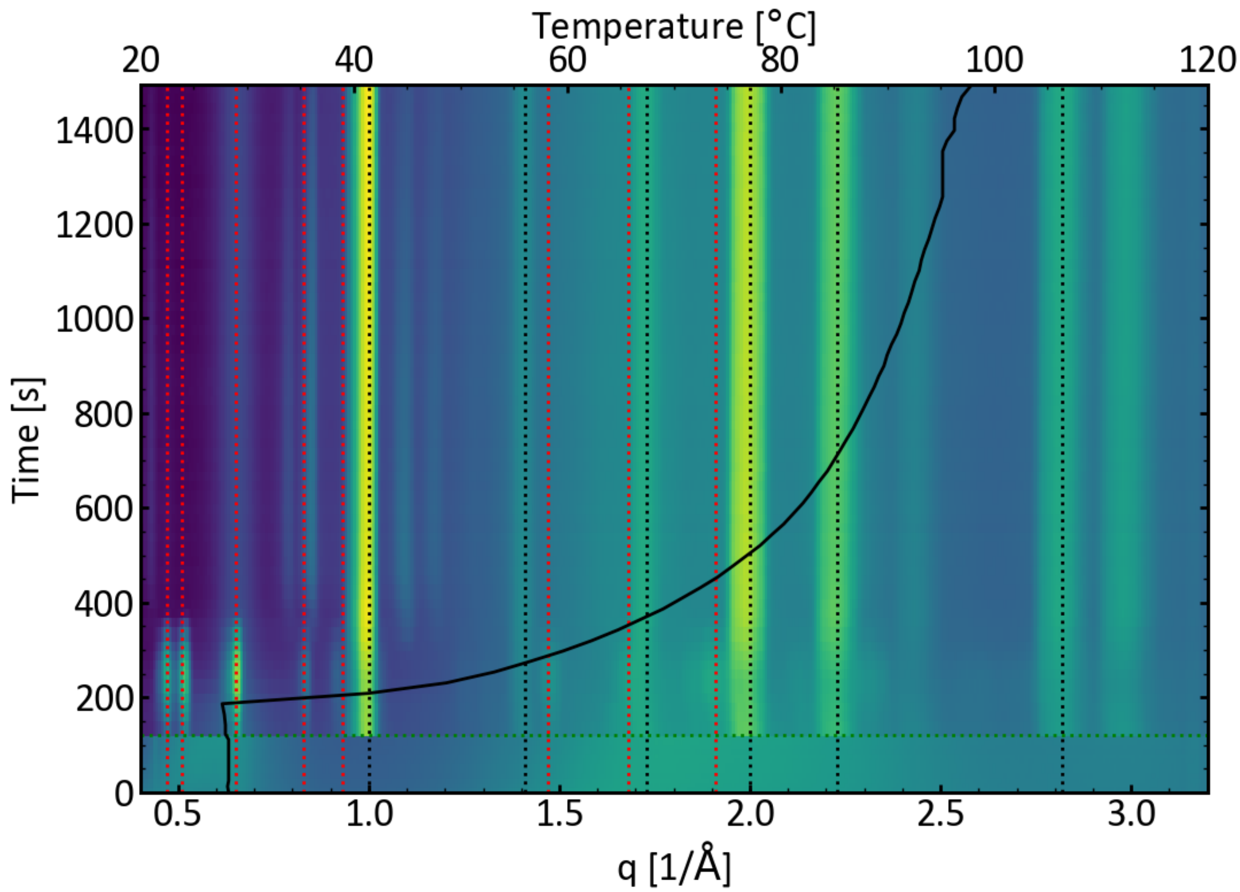

Figure S16 | *In situ* XRD during drying and heating of blade coated film (DMSO, CB added at 2 min). The red and black dashed lines indicate the calculated peak positions for the intermediate and perovskite phase, respectively. The green dashed line marks the addition of chlorobenzene. The solid black line shows the temperature (top abscissa).

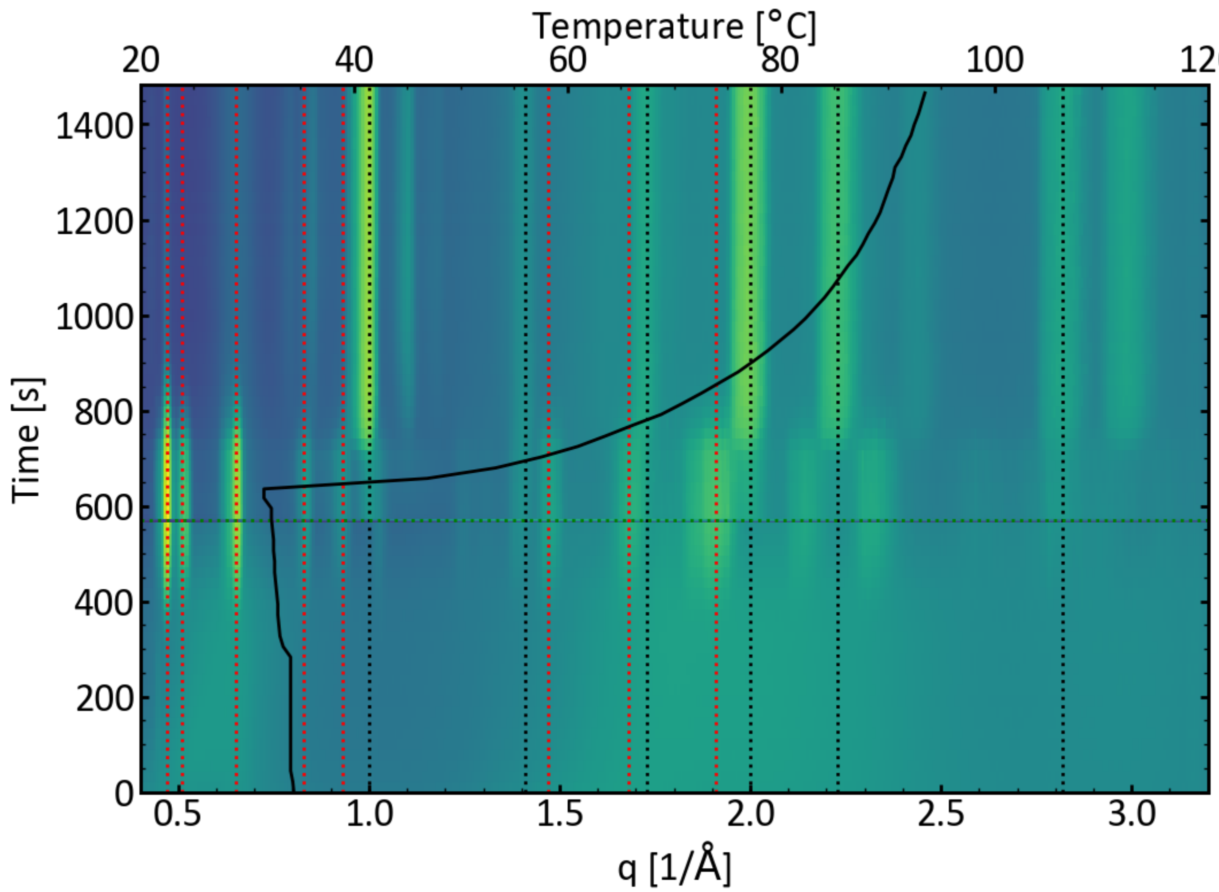

Figure S17 | *In situ* XRD during drying and heating of blade coated film (DMSO, CB added at 10 min). The red and black dashed lines indicate the calculated peak positions for the intermediate and perovskite phase, respectively. The green dashed line marks the addition of chlorobenzene. The solid black line shows the temperature (top abscissa).

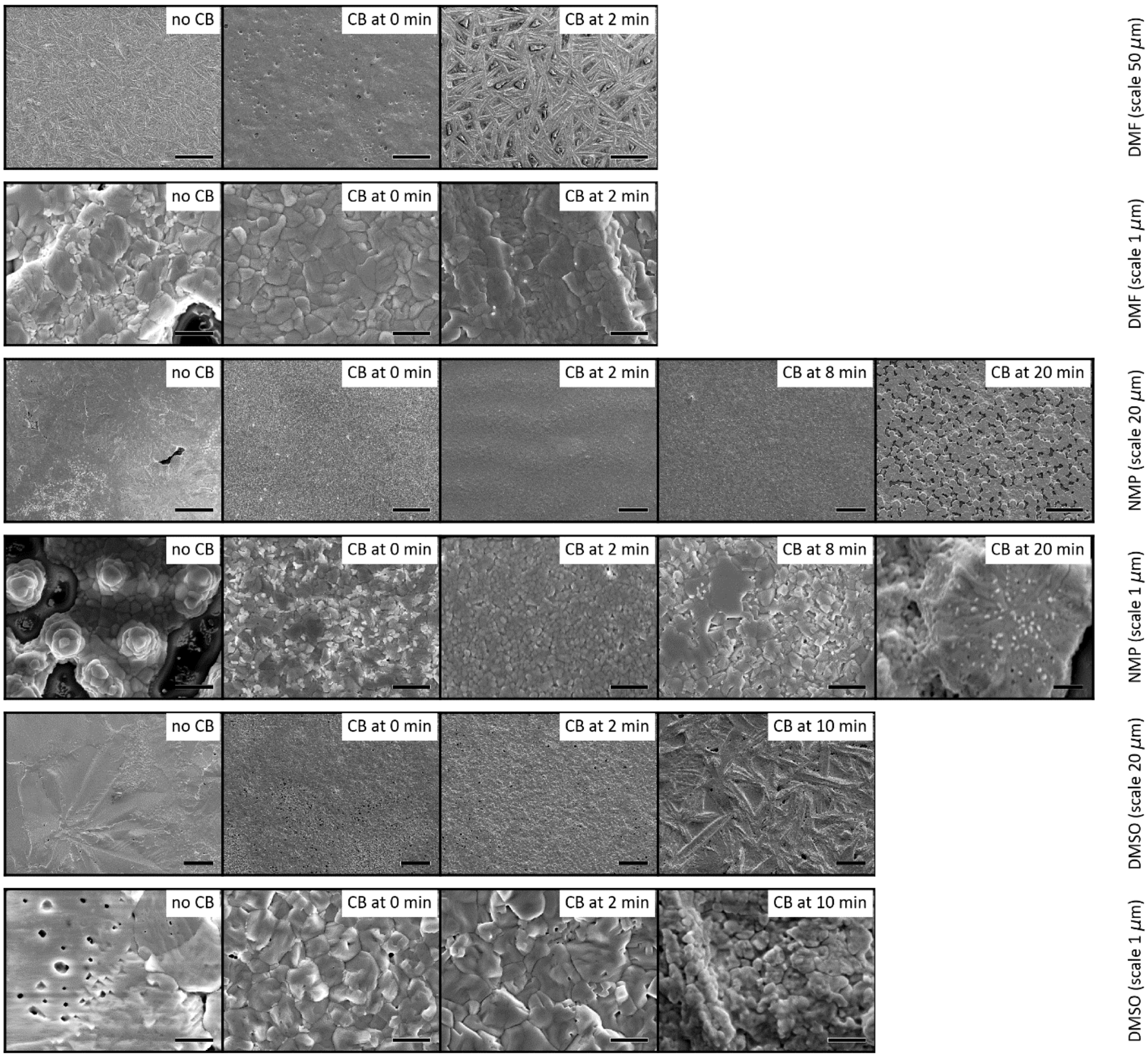

Figure S18 | SEM images of films after the thermal annealing step. The timing of the chlorobenzene addition is indicated in the top right of each image. The solvent system used and the image scale is shown on the right of each row.

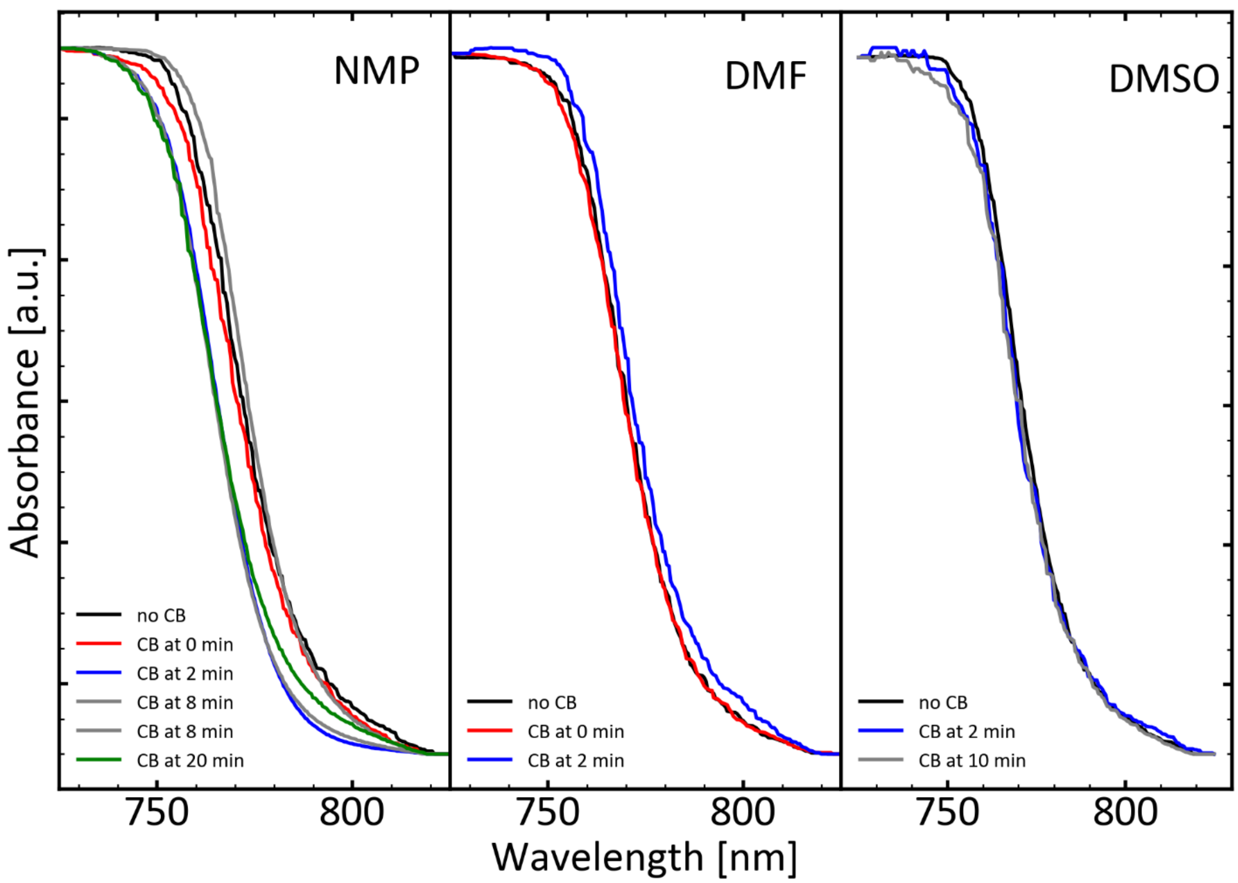

Figure S19 | Normalized UV-vis absorbance spectra of finished films after thermal annealing.

a)

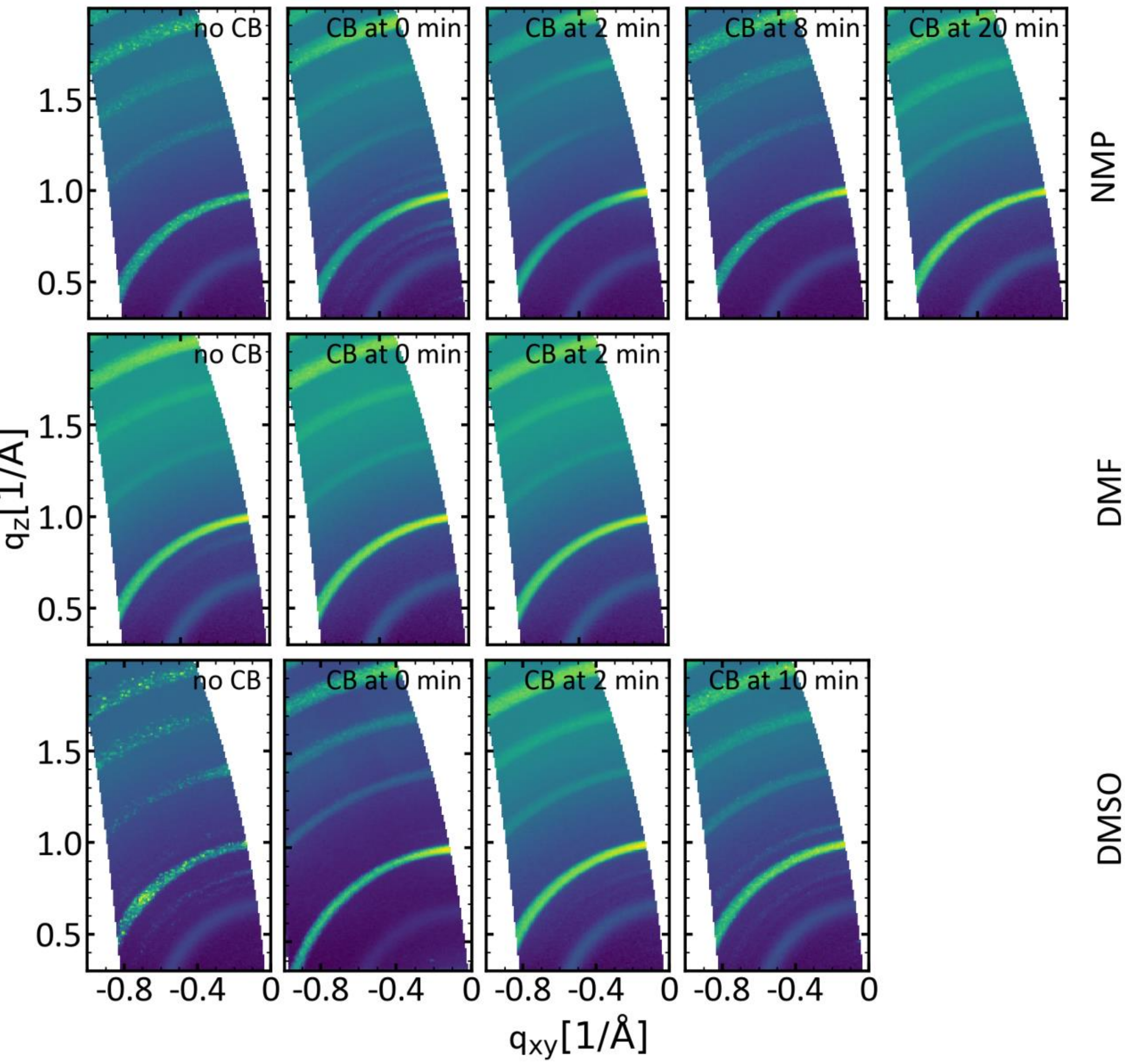
no CB
CB at 0 min
CB at 2 min
CB at 8 min
CB at 20 min
CB at 10 min
NMP
DMF
DMSO
$q_z[1/Å]$
$q_{xy}[1/Å]$
1.5
1.0
0.5
-0.8
-0.4
0

b)

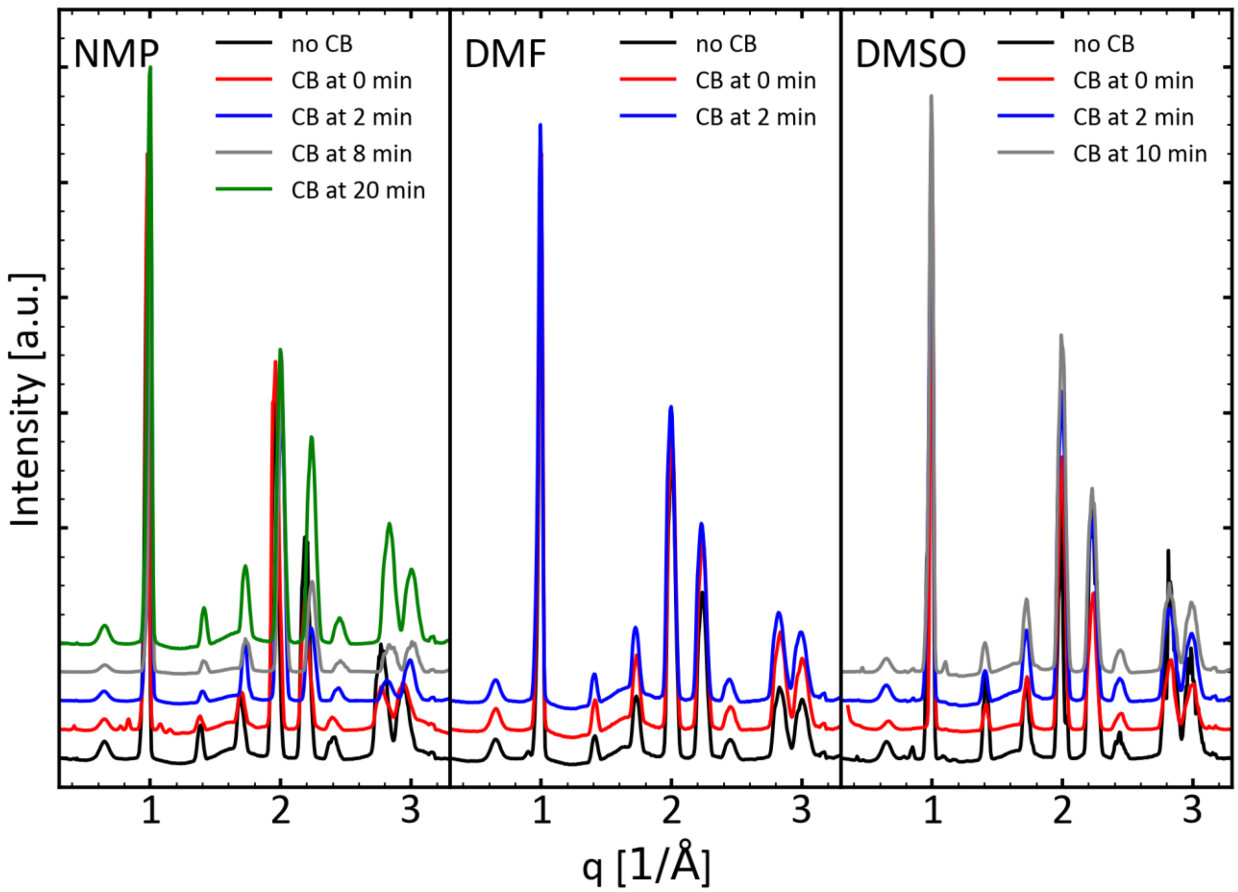

Figure S20 | XRD data for finished films after thermal annealing. **a)** Two-dimensional GIWAXD images represented in $q_{xy} - q_z$ space, **b)** Integrated one-dimensional diffraction curves (vertically shifted). The peak labeled with an asterisk is due to diffraction from the polyimide X-ray window.[13,16,17]

Film Thickness Measurements using Interferometry

The film thickness was measured during blade coating and drying using a Thetametrisis FR-pOrtable interferometer. The refractive indices for DMF, DMSO and NMP for certain wavelengths were obtained from the literature[18] and then fit to the Cauchy equation[19]:

$$n(\lambda) = A + \frac{B}{\lambda^2} + \frac{C}{\lambda^4}$$

with the refractive index n, the wavelength λ and the Cauchy fit parameters A, B, C.The resulting fits are shown in fig. S8.

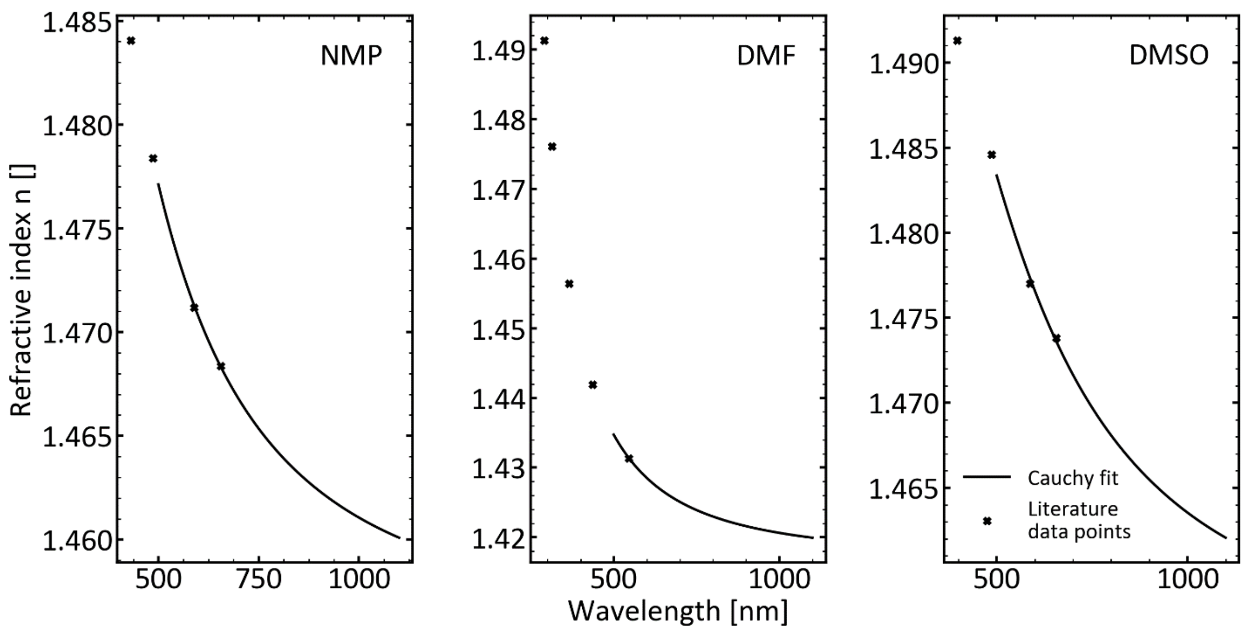

Fig. S21 | Cauchy fits for the refractive indices for NMP, DMF and DMSO (pure solvents).

Next, the refractive indices for the mixed solvents n_{mix} were computed using the Lorentz-Lorenz mixing rule[20] (fig. S9):

$$n_{mix}(a) = \sqrt{\frac{2a+1}{1-a}}$$

$$a = \phi_1 t(n_1) + \phi_2 t(n_2)$$

$$t(n) = \frac{n^2-1}{n^2+2}$$

with the volume fraction ϕ_i for solvent i.

The refractive indices of the solution were assumed to be consistent with those of the mixed solvents, i.e. the contributions of the solutes (and their varying concentration over time) were neglected. For that reason, the reported thicknesses should be interpreted as relative values.

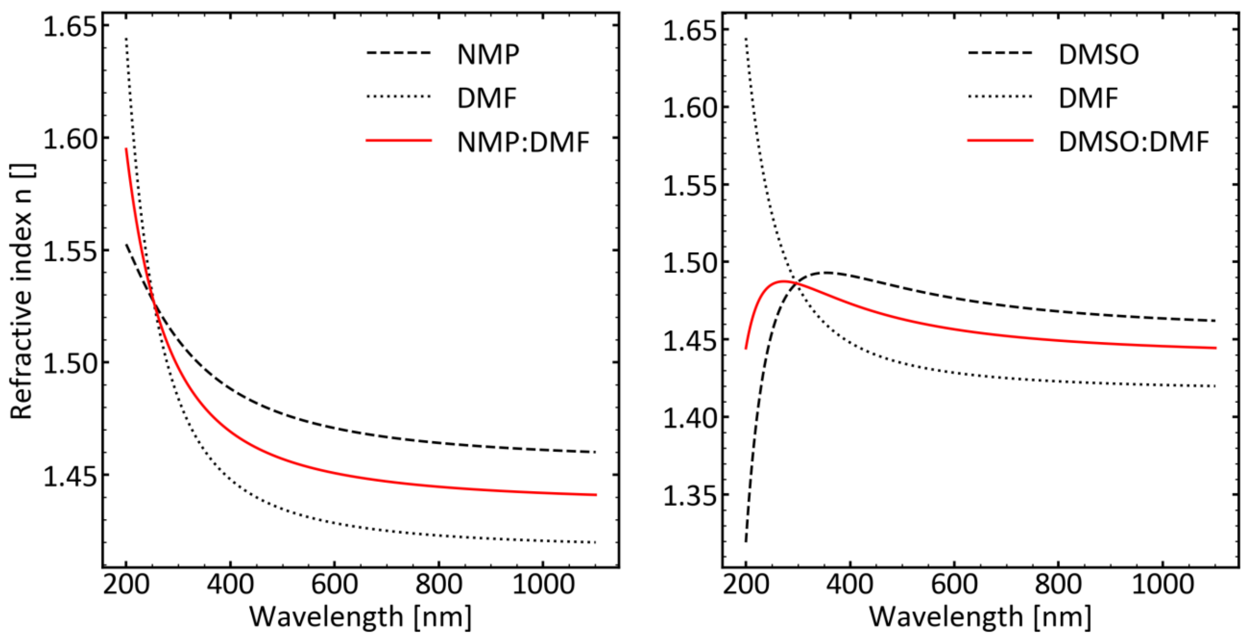

Fig. S22 | Refractive indices for mixed solvents.

References

1 A. Kojima, K. Teshima, Y. Shirai and T. Miyasaka, *JACS*, 2009, **131**, 6050–6051.

2 J.-H. Im, C.-R. Lee, J.-W. Lee, S.-W. Park and N.-G. Park, *Nanoscale*, 2011, **3**, 4088.

3 H.-S. Kim, C.-R. Lee, J.-H. Im, K.-B. Lee, T. Moehl, A. Marchioro, S.-J. Moon, R. Humphry-Baker, J.-H. Yum, J. E. Moser, M. Grätzel and N.-G. Park, *Sci. Rep.*, 2012, **2**, 1–7.

4 J. M. Ball, M. M. Lee, A. Hey and H. J. Snaith, *Energy Environ. Sci.*, 2013, **6**, 1739–1743.

5 J. Burschka, N. Pellet, S.-J. Moon, R. Humphry-Baker, P. Gao, M. K. Nazeeruddin and M. Grätzel, *Nature*, 2013, **499**, 316–9.

6 J. T. W. Wang, J. M. Ball, E. M. Barea, A. Abate, J. a. Alexander-Webber, J. Huang, M. Saliba, I. Mora-Sero, J. Bisquert, H. J. Snaith and R. J. Nicholas, *Nano Lett.*, 2014, **14**, 724–730.

7 D. Liu and T. L. Kelly, *Nat. Photonics*, 2013, **8**, 133–138.

8 Z. Xiao, Q. Dong, C. Bi, Y. Shao, Y. Yuan and J. Huang, *Adv. Mater.*, 2014, **26**, 6503–6509.

9 H. Zhou, Q. Chen, G. Li, S. Luo, T. Song, H.-S. Duan, Z. Hong, J. You, Y. Liu and Y. Yang, *Science (80-.).*, 2014, **345**, 542–547.

10 W. S. Yang, J. H. Noh, N. J. Jeon, Y. C. Kim, S. Ryu, J. Seo and S. I. Seok, *Science (80-.).*, 2015, **348**, 1234–1237.

11 M. Saliba, T. Matsui, J.-Y. Seo, K. Domanski, J.-P. Correa-Baena, M. K. Nazeeruddin, S. M. Zakeeruddin, W. Tress, A. Abate, A. Hagfeldt and M. Grätzel, *Energy Environ. Sci.*, 2016, **9**, 1989–1997.

12 W. S. Yang, B. Park, E. H. Jung and N. J. Jeon, *Science (80-.).*, 2017, **356**, 1376–1379.

13 A. A. Petrov, I. P. Sokolova, N. A. Belich, G. S. Peters, P. V Dorovatovskii, Y. V Zubavichus, V. N. Khrustalev, V. Petrov, M. Grätzel, E. A. Goodilin and A. B. Tarasov, *J. Phys. Chem. C*, 2017, **121**, 20739–20743.

14 H. Tanaka and E. Nakamura, *J. Am. Chem. Soc.*, 2015, **137**, 15907–15914.

15 Y. Rong, Z. Tang, Y. Zhao, X. Zhong, S. Venkatesan, H. Graham, M. Patton, Y. Jing, A. M. Guloy and Y. Yao, *Nanoscale*, 2015, **7**, 10595–10599.

16 M. Ree, T. L. Nunes and J. S. Lin, *Polymer (Guildf).*, 1993, **35**, 1148–1156.

17 T. Tanaka, Y. Inuishi, J. Sunada, K. Oishi, A. Kasai, S. Ehara and K. Muramatsu, *Jpn. J. Appl. Phys.*, 1986, **25**, 1542–1545.

18 C. Wohlfarth and B. Wohlfarth, *Refractive Indices of Organic Liquids, Datasheet from Landolt-Börnstein - Group III Condensed Matter, Volume 38B*, Springer-Verlag, Berlin, Heidelberg, 1996.

19 F. A. Jenkins and H. E. White, *Fundamentals of Optics*, McGraw-Hill, New York, 4th edn., 1976.

20 A. Tasic, B. D. Djordjevic, D. K. Grozdanic and M. Radojkovic, *J. Chem. Eng. Data*, 1992, **37**, 310–313.